Electronic Supporting Information (ESI)

A Cu^{I}/Cu^{II} mixed-valence metal-organic framework for CO_2 conversion

Yu-Mei Wang,[‡a,b] Kai-Ming Mo,[‡a] Dong Luo,[a] Mei-Xia Tao,[a] Xu Chen,[a] Guo-Hong Ning*[a] and Dan Li*[a]

[a] College of Chemistry and Materials Science, Guangdong Provincial Key Laboratory of Supramolecular Coordination Chemistry, Jinan University, Guangzhou, Guangdong 510632, China

[b] Jiangxi Provincial Key Laboratory of Functional Crystalline Materials Chemistry, Jiangxi University of Science and Technology, Jiangxi, Ganzhou 341000, China

E-mail: guohongning@jnu.edu.cn; danli@jnu.edu.cn

Table of Contents

1. General Method

All chemicals and solvents were purchased and used without further purification. Single crystal diffraction data by XtaLAB AFC12 (RINC) single crystal diffractometer was then collected under 100 K. The light source of the single crystal diffractometer adopts Cu-Kα (λ = 1.54184) monochromatized by a graphite monochromator. Powder X-ray diffraction (PXRD) data was collected at 40 kV, 30 mA using microcrystalline samples on a Rigaku Ultima IV diffractometer using Cu-Kα radiation (λ = 1.5418 Å). The measurement parameters include a scan speed of 0.5°/min, a step size of 0.02°, and a scan range of 2θ from 3° to 40°. Thermogravimetric analysis was performed on a Mettler-Toledo (TGA/DSC1) thermal analyzer. Measurement was made on approximately 5 mg of dried samples under a N_2 flow with a heating rate of 10 °C/min from 40 ℃ to 800 ℃. X-ray photoelectron (XPS) spectroscopy spectra were performed by a Thermo ESCALAB 250XI system. Liquid ^{1}H and ^{13}C NMR spectra were recorded on a Bruker Biospin Avance (400 MHz) equipment using tetramethylsilane (TMS) as an internal standard. The following abbreviations were used to explain the multiplicities: s = singlet, d = doublet, t = triplet, q = quartet, dd = doublet of doublet, dt = doublet of triplet, m = multiplet, Flash column chromatography was performed using Merck silica gel 60 with commercially available solvents.

2. Synthesis and characterization of H_2L and 1

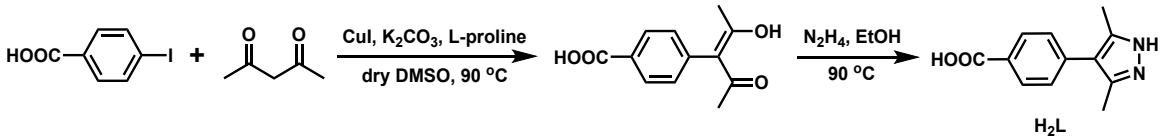

Scheme S1. Synthetic route of ligand $\mathbf{H_2L}$.

3,5-dimethyl-4-(4-carboxyphenyl)-1H-pyrazole ($\mathbf{H_2L}$) was prepared according to reported procedures.[1]

Synthesis of the intermediate 3-(4-carboxyphenyl)-2,4-pentanedione: 4-Iodobenzoic acid (2.5 g, 10 mmol), copper(I) iodide (0.2 g, 1 mmol), L-proline (0.25 g, 2 mmol) and K_2CO_3 (5.5 g, 40 mmol) were suspended in dry dimethyl sulfoxide (80 mL) and stirred for 10 minutes at room temperature. 2,4-Pentanedione (3.1 mL, 30 mmol) was slowly added dropwise to the mixture and the initially blue mixture turned green within five minutes. The suspension was heated to 90 °C and stirred for 24 hours. After the mixture was cooled to room temperature, it was slowly transferred into hydrochloric acid (3 mol/L, 500 mL) with vigorous stirring. An additional 300 mL of water was added to the suspension and cooled in an ice bath. A large amount of solid was observed to precipitate. After filtration and washing with ice-cooled water, the filter cake was dried over night at 80 °C in vacuum to afford the the target compound (1.4 g, 6.4 mmol, 64 % based on 4- iodobenzoic acid) as off-white solid. ^{1}H NMR (400 MHz, DMSO-d_6, 298 K): δ [ppm] = 13.14 (s, 1H), 7.89 (d, J = 8.1 Hz, 2H), 7.69 (d, J = 8.2 Hz, 2H), 2.17 (s, 3H), 1.87 (s, 3H).

Synthesis of 3,5-dimethyl-4-(4-carboxyphenyl)-1H-pyrazole ($\mathbf{H_2L}$). A solution of 3-(4-carboxyphenyl)-2,4-pentanedione (1.4 g, 6.4 mmol) in ethanol (20 mL) was heated at 90 °C, 3 mL hydrazine monohydrate (80% in water) in ethanol (20 mL) was slowly added dropwise to the mixture and and the reaction continued for 3 hours. After cooling to room temperature the solution was concentrated under reduced pressure to one third of the original volume. The residue was slowly added dropwise to 400 mL of ice water, and the pH of the solution was adjusted to 6-7 with dilute hydrochloric acid. A large amount of solid precipitation was observed. The precipitate was filtered and washed three times with ice-cooled water and dried in vacuum over night at 80 °C to afford compound $\mathbf{H_2L}$ (1.2 g, 5.5 mmol, 86 % based on 3-(4-carboxyphenyl)-2,4-pentanedione) as a white solid. ^{1}H

NMR (400 MHz, DMSO-d_6, 298 K): δ [ppm] = 13.00 (s, 1H), 7.89 (d, J = 7.9 Hz, 2H), 7.69 (d, J = 8.0 Hz, 2H), 2.24 (s, 6H).

Caution! The volume of solution should not exceed half of the volume of Pyrex tube to avoid overloading in solvothermal synthesis.

Synthesis of complex 1. A mixture of $Cu(NO_3)_2 \cdot 3H_2O$ (5.8 mg, 0.04 mmol), **H_2L** (9.7 mg, 0.045 mmol), 0.1 M HCl (0.05 mL), N,N-dimethylformamide (1.5 mL) and mesitylene (1.5 mL) was sealed in a Pyrex glass tube, and then the resulting mixture was heated in an oven at 80 °C for 72 hours. Afterward the mixture was cooled to rt with a cooling rate of 5 °C per hour to produce **1** as light green crystal (10.3 mg, yield 90 %, based on Cu). IR (KBr): 3435 (w), 2916 (w), 1654 (m), 1608 (m), 1560 (w), 1541 (m), 1493 (w), 1402 (m), 1181 (s), 1034 (m), 1015 (m), 864 (s), 781 (m), 713 (w) cm^{-1}.

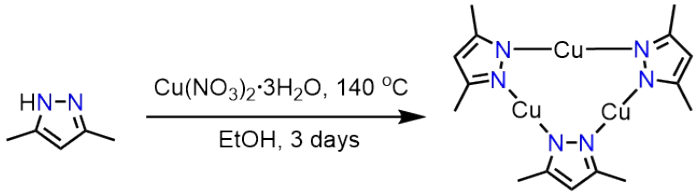

Scheme S2. Synthetic route of complex **2**.

Synthesis of reference complex 2.[2] Complex **2** was prepared according to reported procedures with slight modification.[2] 3,5-dimethylpyrazole (96 mg, 1.0 mmol) and $Cu(NO_3)_2 \cdot 3H_2O$ (120.8 mg, 0.5 mmol) were dissolved in a mixture of EtOH/chlorobenzene (2/1 v/v, 3 mL). The mixture was sealed in a Pyrex tube and heated at 140 °C for 72 h in an oven. Slowly cooling to rt, complex **2** as yellowish block crystals could be obtained. Yield: 65% based on Cu.

Synthesis of HKUST-1 followed the described procedure.[3] Trimesic acid (504 mg, 2.4 mmol) and $Cu(NO_3)_2 \cdot 3H_2O$ (1038 mg, 4.3 mmol) were placed in a 100 mL Schlenk flask. A mixture of solvents (30 mL), which was prepared at a volume ratio of 1:1:1 of each solvent (DMF-EtOH-H2O), was added to the flask and sonicated for 10 min. The Schlenk flask was placed in an oven at 85°C for 20 hours, then the blue crystals formed at the bottom of the flask are **HKUST-1**.

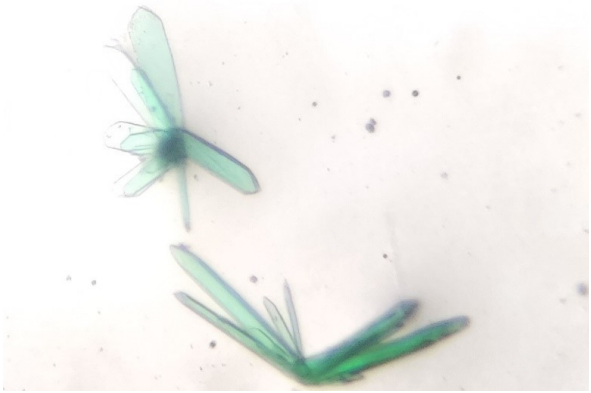

Fig. S1 Photograph of as-synthesized crystals of **1**.

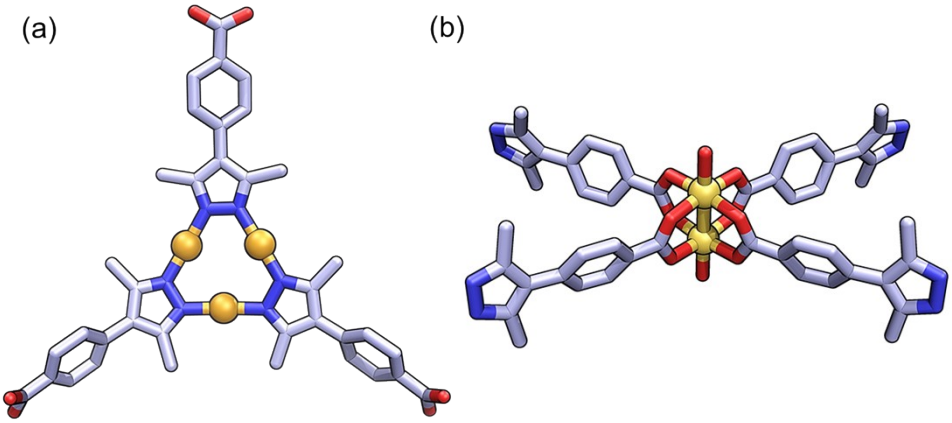

Fig. S2 The structural units formed by the coordination of $\mathbf{H_2L}$ with Cu^{I} and Cu^{II} in the structure of **1**.

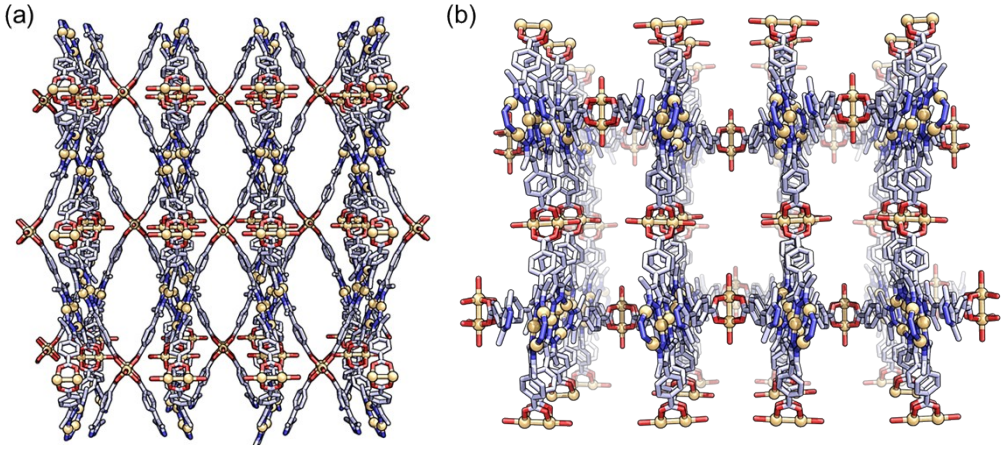

Fig. S3 Perspective view of the 3D structure of the **1** along the (a) b- and (b) c-axes.

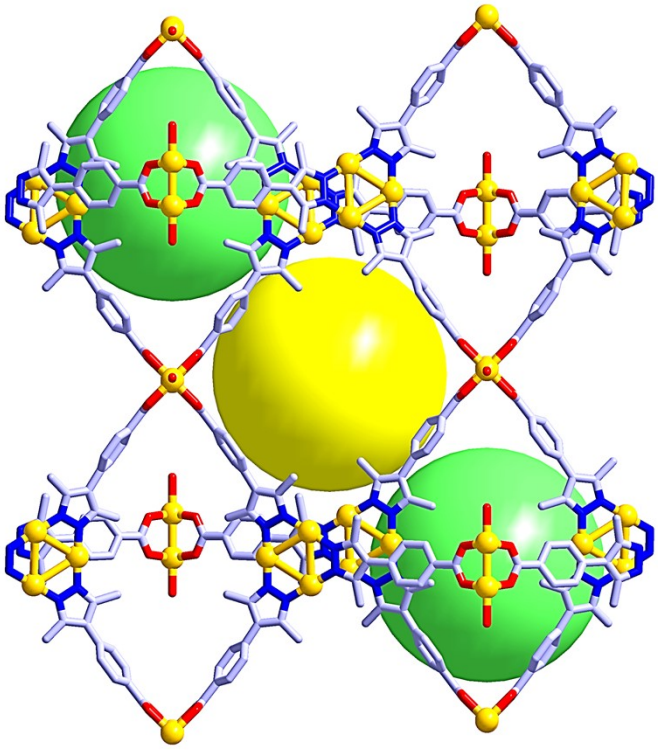

Fig. S4 The structure of **1** has a three-dimensional cage-like network with different porous channels along crystallographic a-axis. The yellow and green solid balls both have a diameter of 15 Å.

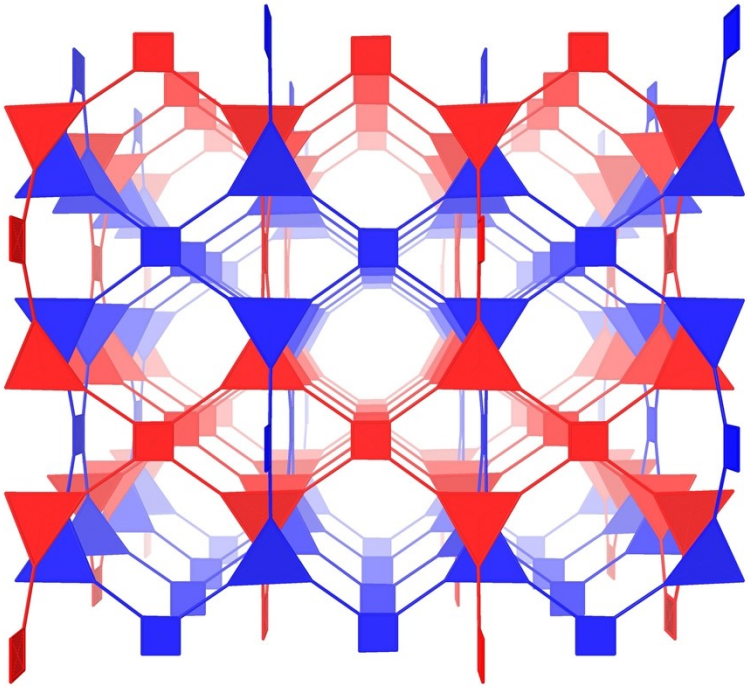

Fig. S5 2-interpenetrated structure of **1** following a simplified topology.

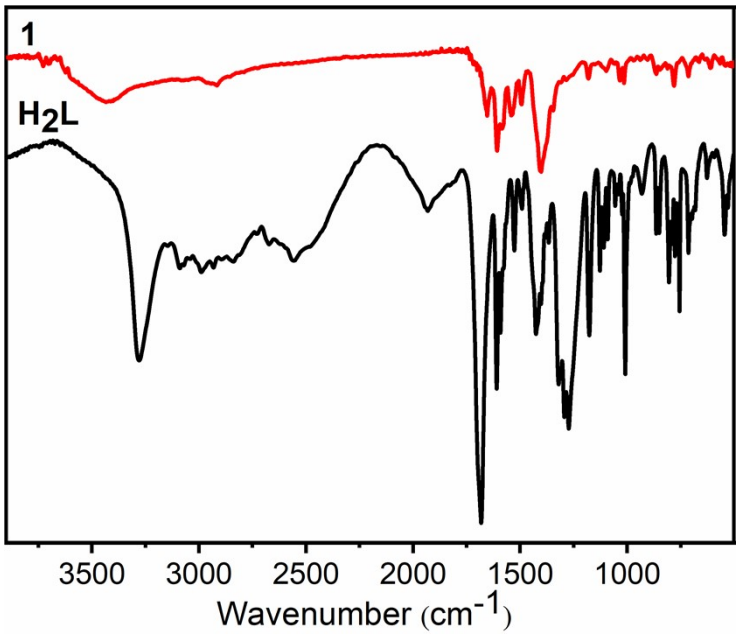

Fig. S6 FT-IR spectra of **H_2L** and **1**.

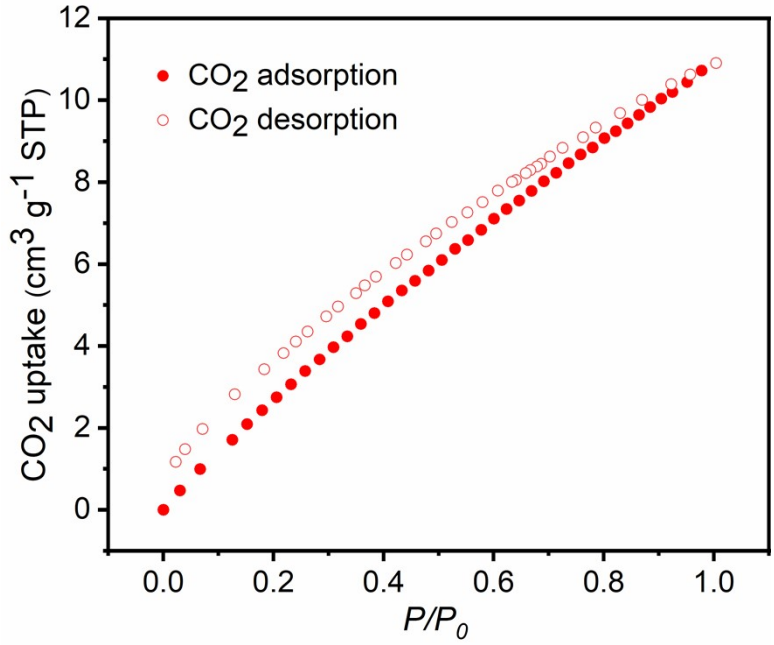

Fig. S7 CO_2 adsorption/desorption isotherms of activated **1** at 298 K.

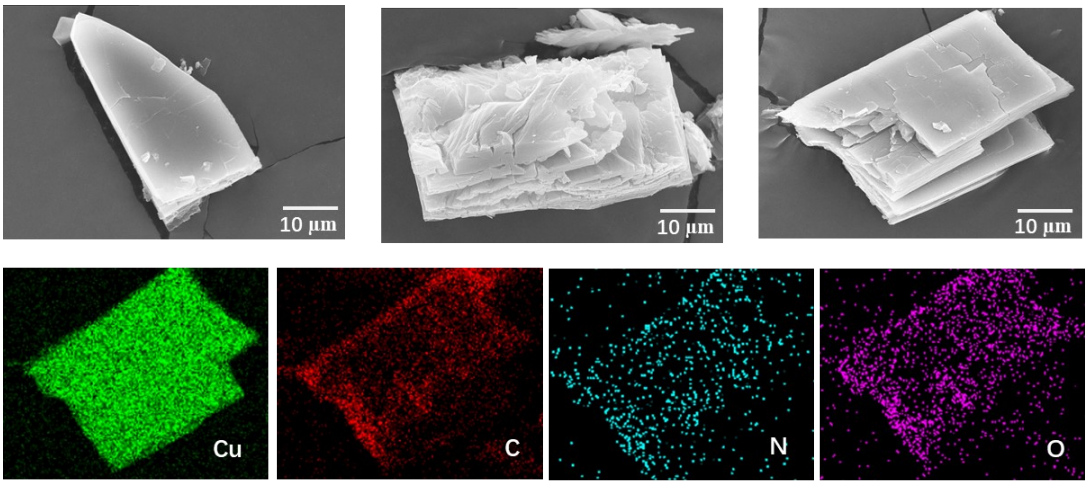

Fig. S8 The SEM image and EDS of **1**.

3. Single Crystal X-ray diffraction analysis of 1

Suitable single crystals of **1** were mounted with nylon loops. Data was collected on an Oxford Diffraction XtalAB [Rigaku (Cu) Xray dual wavelength source, Kα, λ = 1.5418 Å] equipped with a monochromator and CCD plate detector (CrysAlisPro CCD, Oxford Diffraction Ltd) at 100 K. The structure was solved by direct methods and refined by full-matrix least-squares refinements based on F^2.[4-7] Single-crystal structures of compounds **1** were solved by direct methods by ShelXS in Olex2 1.2. All non-hydrogen atoms were refined with anisotropic thermal parameters, and all hydrogen atoms were included in calculated positions and refined with isotropic thermal parameters riding on those of the parent atoms. Crystal data and structure refinement parameters were summarized in Table S1. CCDC Number 2336501 (**1**), contain the supplementary crystallographic data for this paper. Topology information for **1** was calculated by TOPOS 4.0.35. *Systre* [8] program and the commercial software *CrystalMaker X* were used to identify the underlying net of MOFs and to generate/process the .cgd file for the nets. *ToposPro*[9] program was used for computing point symbol and vertex symbol[10] of the net. The *RCSR* (Reticular Chemistry Structure Resource)[11] and *Topcryst* (The Samara Topological Data Center)[12] online databases can be used for searching nets and checking their occurrences in crystal structures.

Table S1. Crystal data for **1**

Parameter	**1**
CCDC Number	2336501
Chemical formula	$(C_{48}\ H_{44}\ Cu_6\ N_8\ O_{10})_n$
Formula weight	952.59
Temperature (K)	100.01(12)
Crystal system	orthorhombic
Space group	*Cmcm*
a (Å)	26.5883(19)
b (Å)	41.9586(14)
c (Å)	37.5283(16)
α (deg)	90
β (deg)	90
γ (deg)	90)
V (Å^3)	41867(4)
Z	16
ρ_{calcd} (g cm^{-3})	0.605
μ (mm^{-1})	1.192
F(000)	7656.0
Radiation	CuKα (λ = 1.54184)
2θ range for data collection/°	6.138 to 158.314
Reflections collected	91177
Independent reflections	22579 [R_{int} = 0.1059， R_{sigma}= 0.1042]
Data/restraints/parameters	22579/0/506
Goodness-of-fit on F^2	0.885
R_1[a], wR_2[b] [I > 2σ (I)]	R_1=0.0853, wR_2=0.2177
R_1[a], wR_2[b] (all data)	R_1=0.1354, wR_2=0.2478
Largest diff. peak/hole / e Å^{-3}	0.76/-0.43

[a] $R_1 = \Sigma||F_0| - |F_c||/\Sigma|F_0|$. [b] $wR_2 = \{[\Sigma w(F_0^2 - F_c^2)^2]/\Sigma[w(F_0^2)^2]\}^{1/2}$; $w = 1/[\sigma^2(F_0^2) + (aP)^2 + bP]$, where $P = [\max(F_0^2,0) + 2F_c^2]/3$.

4. The cyclization reactions of epoxides with CO_2.

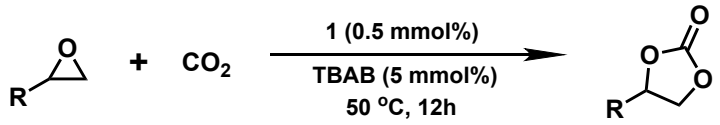

Scheme S3. General procedure for cyclization reaction of epoxides amine and CO_2.

General procedures for cyclization reaction of epoxides and CO_2 by 1: Added 1 mmol epoxides compound, 0.5 mmol% **1** and 0.05 mmol tetrabutylammonium bromide (TBAB) into the Schlenk bottle, and mixed evenly. The air in the Schlenk bottle was removed to maintain a vacuum, 1 atm carbon dioxide was introduced into the Schlenk bottle, and the reaction mixture was stirred at 50 ℃ for 12 hours. The subsequent experimental process was same as the previous reaction.

Table S2. TOF comparison between **1** and previously reported MOFs catalysts for cyclization reaction of epoxides and CO_2

Entry	Catalysts	P (atm)	T (℃)	t (h)	TOF(h^{-1})	Ref.
1	**1**[a] [b] / **1**[a] [c]	1	50	12	16.7 / 2.8	This work
2	JNM-15[b]	2	55	6	82.5	13
3	JNM-14[b]	2	55	6	78.3	13
4	JNM-13[b]	2	55	6	70.8	13
3	Cu^{II} MOF[c]	1	rt	48	88.5	14
4	Cu^{II} MOF[c]	1	rt	48	5.0	15
5	Cu^{II} MOF[b]	8	70	6	115.5	16
6	JLU-Liu21[c]	1	80	48	7.7	17
7	Cu^{II} MOF[b]	1	60	12	20.6	18

8	Cu^{II} MOF[b]	12	60	12	32	19
9	Cu^{II} MOF[b]	1	90	24	20.2	20
10	Cu-URJC-8[b]	12	25	24	3.7	21
11	Cd-MOF-**1**[b]	1	80	16	16.4	22
12	HbMOF1[b]	1	30	24	41.5	23
13	Mn-MOF[b]	1	rt	20	8.3	24
14	Zr-MOF[b]	1	100	4	49.7	25
15	NUC-5[b]	1	80	24	2.7	26
16	NUC-21[b]	1	60	6	8.3	27
17	Zn_2(oxdia) (4,4′-bpy)$_2$[b]	1	28	16	25.0	28
18	Zn-2PDC[b]	10	55	12	1.7	29
19	Cu_2(4-TPOM) (3,7-DBTDC[b]	1	28	24	24.5	30
20	[Zn_2(TPOM) (L_2)][b]	1	40	16	11.9	31
21	Cd-MOF[b]	1	50	12	206.25	32
22	Cu^{I}/Cu^{II} MOF[b]	1	90	5	28.6	33
23	CdMOF-2[b]	1	45	24	3.5	34

TOF is calculated directly using the optimal conditions given in the literature. [a] Reaction condition: 1 mmol substrate, 4.8 mg compound **1** (0.005 mmol, 0.03 mmol based on Cu), 1 atm CO_2, and solvent free. 12 hours after the reaction, the yield determinned by ^{1}H NMR with 1,1,2,2-tetrachloroethane as the internal standard.
TOF: Turnover frequency was evaluated at optimal conditions and calculated by the mole number of product per mole number of [b]catalysts or [c]catalytic metal active per hour.

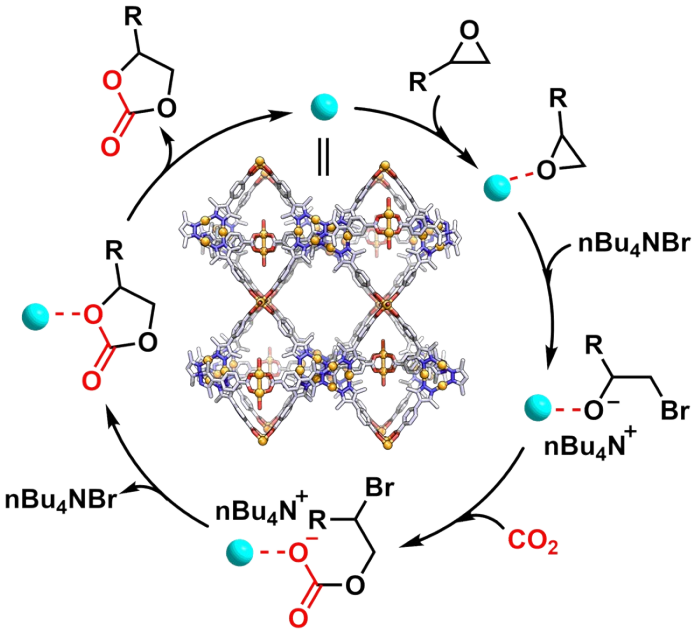

Fig. S9 Proposed reaction mechanism for the cyclization reaction of epoxides and CO_2 catalyzed by **1**.

5. The cyclization reactions of propargylic amines with CO_2.

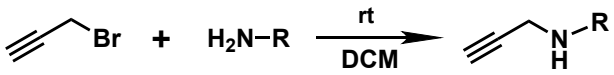

Scheme S4. General procedure for the synthesis of terminal propargylic amine (3a-3e).

General procedures for the synthesis of terminal propargylic amine: Propargylic bromide (10 mmol) was slowly added into the benzylamine compound (50 mmol) in dichloromethane (20 mL) via a constant pressure drop funnel over thirty minutes, and the reaction solution was stirred at room temperature for 12 hours. The reaction mixture was extracted three times with dichloromethane and aq. $NaHCO_3$, and the organic layer solution was collected and dried over anhydrous Na_2SO_4. The reaction mixture was concentrated and purified by column chromatography on silica gel eluting with 10:1 petroleum ether/ethyl acetate to afford the corresponding product as pale-yellow liquid.

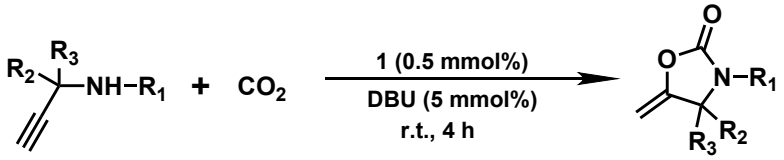

Scheme S5. General procedure for cyclization reaction of propargylic amine and CO_2.

General procedure for the cyclization reaction of propargylic amine and CO_2 catalyzed by 1: Added 0.5 mmol propargylic amine compound, 0.5 mmol% **1** and 0.025 mmol 1,8-Diazabicyclo[5,4,0]-undec-7-ene (DBU) into the Schlenk bottle, and mixed evenly. The air in the Schlenk bottle was removed to maintain a vacuum, 0.1 MPa carbon dioxide was introduced into the Schlenk bottle, and the reaction mixture was stirred at room temperature for 4 hours. The mixture was rinsed with dichloromethane, filtered and collected the catalyst and filtrate. After removing the solvent from the filtrate under reduced pressure, 0.5 mmol 1,1,2,2-tetrachloroethane was added as an internal standard, and the yield was calculated by ^{1}H NMR. Finally, it was purified by flash column chromatography on silica gel (petroleum ether: ethyl acetate = 15: 1) to afford desired pure products. Different catalysts, solvents, and others were investigated in a similar procedure.

Table S3. TOF comparison between **1** and previously reported MOFs catalysts for cyclization reaction of propargylic amine and CO_2.

Entry	Catalysts	P (atm)	T (°C)	Solvent	t (h)	TOF(h^{-1})	Ref.
1	**1**[a] [b] / **1**[a] [c]	1	rt	--	10	142.8 / 23.8	This work
2	WYU-11[b]	1	60	CH_3CN	24	4.1	35
3	Cu_2O@ZIF-8[c]	1	40	CH_3CN	6	3.3	36
4	$[Zn_{116}]$-MOF[b]	1	70	CH_3CN	12	30.5	37
5	TMOF-3-Ag[b]	1	50	DMSO	6	1.7	38
6	$[Cu_2I_2]$-Eu-MOF[b]	1	70	--	12	10.2	39
7	CuBr@NH_2-MIL-101[c]	1	rt	CH_3CN	8	2.4	40
8	Cu^I/Cu^{II} MOF[c]	1	30	--	0.17	230	41

TOF is calculated directly using the optimal conditions given in the literature. [a] Reaction condition: 1.2 g (8.3 mmol) substrate, 4.8 mg compound **1** (0.005 mmol 0.03 mmol based on Cu), 1 atm CO_2, and solvent free. 10 hours after the reaction, the yield determinned by ^{1}H NMR with 1,1,2,2-tetrachloroethane as the internal standard.
TOF: Turnover frequency was evaluated at optimal conditions and calculated by the mole number of product per mole number of [b]catalysts or [c]catalytic metal active per hour.

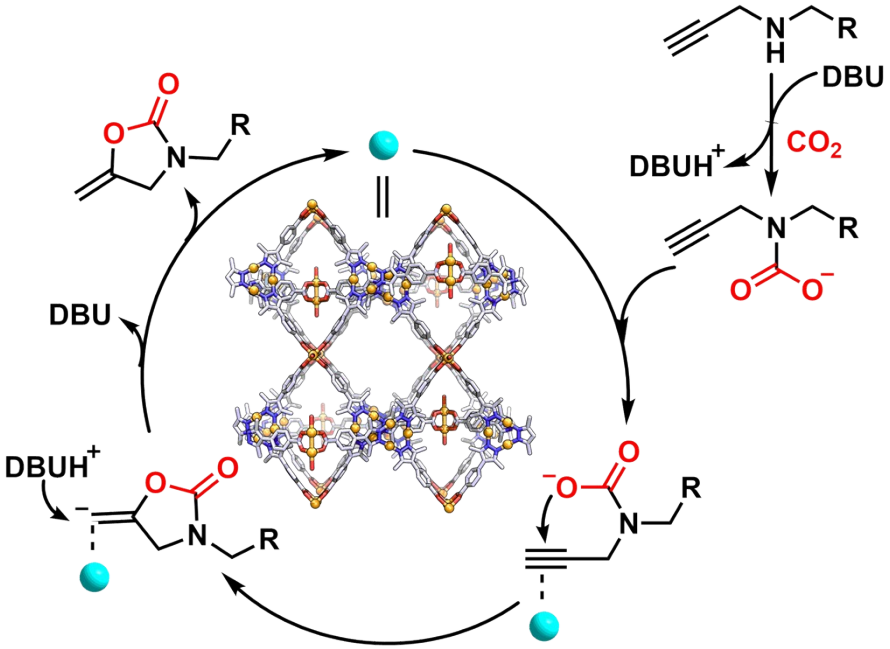

Fig. S10 Proposed reaction mechanism for the cyclization reaction of propargylic amine and CO_2 catalyzed by **1**.

6. Reusability of catalyst 1

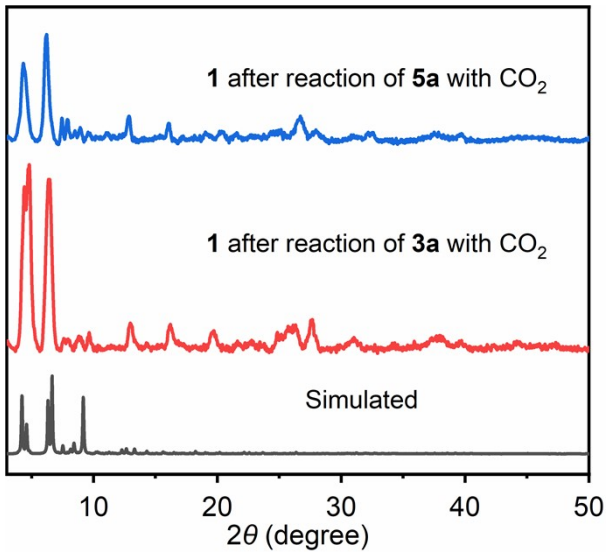

Fig. S11 PXRD spectrum comparison of simulated (black) and recovered **1** after catalyst for cyclization reaction of epoxides and CO_2 (red) and cyclization reaction of propargyl amine and CO_2.

7. Characterization of compounds 4 and 6

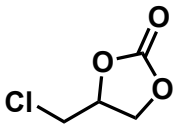

4-(chloromethyl)-1,3-dioxolan-2-one (4a); ^{1}H NMR (400 MHz, $CDCl_3$, 298 K) δ [ppm] = 5.13 – 4.82 (m, 1H), 4.55 (t, *J* = 8.6 Hz, 1H), 4.34 (dd, *J* = 8.9, 5.7 Hz, 1H), 3.74 (ddd, *J* = 41.9, 12.4, 4.1 Hz, 2H). ^{13}C NMR (101 MHz, $CDCl_3$, 298 K) δ [ppm] = 154.82, 74.80, 67.22, 44.48.

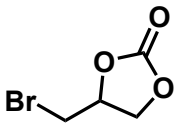

4-(bromomethyl)-1,3-dioxolan-2-one (4b); ^{1}H NMR (400 MHz, $CDCl_3$, 298 K) δ [ppm] = 5.09 – 4.84 (m, 1H), 4.58 (td, *J* = 8.5, 2.6 Hz, 1H), 4.33 (dq, *J* = 8.6, 4.1 Hz, 1H), 3.75 – 3.40 (m, 1H). ^{13}C NMR (101 MHz, $CDCl_3$, 298 K) δ [ppm] = 154.35, 74.10, 68.14, 31.83.

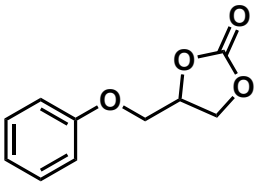

4-(phenoxymethyl)-1,3-dioxolan-2-one (4c); ^{1}H NMR (400 MHz, $CDCl_3$, 298 K) δ [ppm] = 7.30 (t, *J* = 7.8 Hz, 2H), 7.01 (t, *J* = 7.3 Hz, 1H), 6.90 (d, *J* = 8.1 Hz, 2H), 5.04 – 4.98 (m, 1H), 4.59 (t, *J* = 8.4 Hz, 1H), 4.55 – 4.47 (m, 1H), 4.24 (d, *J* = 3.9 Hz, 1H), 4.12 (dd, *J* = 10.5, 3.4 Hz, 1H). ^{13}C NMR (101 MHz, $CDCl_3$, 298 K) δ [ppm] = 157.85, 154.88, 129.75, 122.00, 114.68, 74.33, 66.95, 66.27.

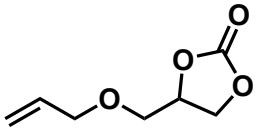

4-((allyloxy)methyl)-1,3-dioxolan-2-one (4d); ^{1}H NMR (400 MHz, $CDCl_3$, 298 K) δ [ppm] = 5.85 – 5.75 (m, 1H), 5.25 – 5.10 (m, 2H), 4.78 (td, *J* = 9.4, 3.4 Hz, 1H), 4.44 (t, *J* = 8.4 Hz, 1H), 4.31 (dd, *J* = 8.3, 6.1 Hz, 1H), 3.98 (dd, *J* = 5.7, 1.7 Hz, 2H), 3.68 – 3.45 (m, 2H). ^{13}C NMR (101 MHz, $CDCl_3$, 298 K) δ [ppm] = 155.51, 155.05, 133.71, 117.55, 75.19, 72.34, 68.81, 66.16.

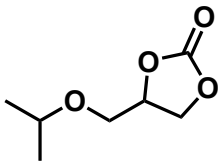

4-(isopropoxymethyl)-1,3-dioxolan-2-one (4e); ^{1}H NMR (400 MHz, $CDCl_3$, 298 K) δ [ppm] = 4.79 – 4.74 (m, 1H), 4.46 (t, *J* = 8.3 Hz, 1H), 4.34 (dd, *J* = 8.3, 6.0 Hz, 1H), 3.72 – 3.44 (m, 3H), 1.12 (d, *J* = 6.2 Hz, 6H). ^{13}C NMR (101 MHz, $CDCl_3$, 298 K) δ [ppm] = 155.22, 75.33, 72.95, 67.16, 66.47, 21.92, 21.81.

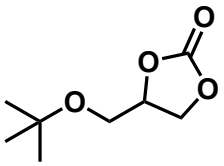

1,4-bis(4-bromophenyl)buta-1,3-diyne (4f); ^{1}H NMR (400 MHz, $CDCl_3$, 298 K) δ [ppm] = 4.79 – 4.69 (m, 1H), 4.44 (t, *J* = 8.2 Hz, 1H), 4.33 (dd, *J* = 8.2, 6.7 Hz, 1H), 3.70 – 3.33 (m, 1H), 1.15 (s, 9H). ^{13}C NMR (101 MHz, $CDCl_3$, 298 K) δ [ppm] = 155.30, 75.33, 73.82, 66.53, 61.29, 27.28.

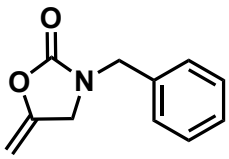

3-benzyl-5-methyleneoxazolidin-2-one (6a); ^{1}H NMR (400 MHz, $CDCl_3$, 298 K) δ [ppm] = 7.41 – 7.25 (m, 5H), 4.74 (d, *J* = 3.0 Hz, 1H), 4.47 (s, 2H), 4.25 (d, *J* = 2.9 Hz, 1H), 4.03 (s, 2H). ^{13}C NMR (101 MHz, $CDCl_3$, 298 K) δ [ppm] = 155.67, 149.02, 135.02, 128.99, 128.26, 128.18, 86.75, 47.82, 47.25.

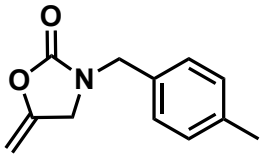

3-(4-methylbenzyl)-5-methyleneoxazolidin-2-one (6b); ^{1}H NMR (400 MHz, $CDCl_3$, 298 K) δ [ppm] = 7.18 (d, *J* = 8.6 Hz, 2H), 6.86 (d, *J* = 8.5 Hz, 2H), 4.69 (q, *J* = 3.1 Hz, 1H), 4.37 (s, 2H), 4.21 (q, *J* = 2.5 Hz, 1H), 3.98 (t, *J* = 2.4 Hz, 2H), 3.78 (s, 3H). ^{13}C NMR (101 MHz, $CDCl_3$, 298 K) δ [ppm] = 7.18 (d, *J* = 8.6 Hz, 2H), 6.86 (d, *J* = 8.5 Hz, 2H), 4.69 (q, *J* = 3.1 Hz, 1H), 4.37 (s, 2H), 4.21 (q, *J* = 2.5 Hz, 1H), 3.98 (t, *J* = 2.4 Hz, 2H), 3.78 (s, 3H).

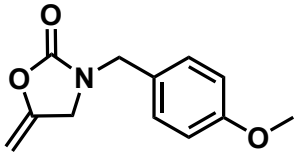

3-(4-methoxybenzyl)-5-methyleneoxazolidin-2-one (6c); ^{1}H NMR (400 MHz, $CDCl_3$, 298 K) δ [ppm] = 7.18 (d, *J* = 4.6 Hz, 2H), 6.86 (d, *J* = 4.1 Hz, 2H), 4.69 (p, *J* = 3.0 Hz, 1H), 4.38 (d, *J* = 3.7 Hz, 2H), 4.24 – 4.17 (m, 1H), 3.99 (d, *J* = 2.3 Hz, 2H), 3.78 (s, 3H). ^{13}C NMR (101 MHz, $CDCl_3$, 298 K) δ [ppm] = 159.56, 155.56, 149.10, 129.60, 127.01, 114.31, 86.61, 55.31, 47.21, 47.09.

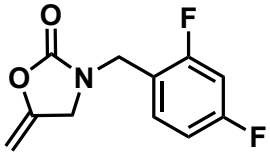

3-(2,4-difluorobenzyl)-5-methyleneoxazolidin-2-one (6d); ^{1}H NMR (400 MHz, $CDCl_3$, 298 K) δ [ppm] = 7.37 – 7.27 (m, 1H), 6.91 – 6.76 (m, 2H), 4.70 (q, *J* = 2.8 Hz, 1H), 4.46 (s, 2H), 4.25 (q, *J* = 2.5 Hz, 1H), 4.08 (s, 2H). ^{13}C NMR (101 MHz, $CDCl_3$, 298 K) δ [ppm] = 159.88, 159.76, 155.45, 148.79, 131.90, 131.85, 131.80, 131.75, 118.31, 118.27, 118.15, 118.12, 112.11, 112.07, 111.90, 111.86, 104.33, 104.07, 103.82, 86.91, 47.50, 40.80

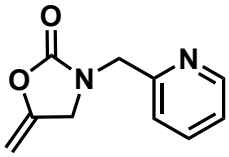

5-methylene-3-(pyridin-2-ylmethyl)oxazolidin-2-one (6e); ^{1}H NMR (400 MHz, $CDCl_3$, 298 K) δ [ppm] = 8.54 (d, *J* = 4.2 Hz, 1H), 7.7 – 7.68 (m, 1H), 7.29 (d, *J* = 7.7 Hz, 1H), 7.22 (dd, *J* = 7.6, 4.9 Hz, 1H), 4.72 (q, *J* = 2.8 Hz, 1H), 4.56 (s, 2H), 4.25 (q, *J* = 2.4 Hz, 1H), 4.22 (t, *J* = 2.4 Hz, 2H). ^{13}C NMR (101 MHz, $CDCl_3$, 298 K) δ [ppm] = 155.85, 155.14, 149.59, 149.17, 137.16, 122.95, 122.29, 86.69, 49.22, 48.12.

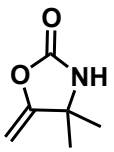

4,4-dimethyl-5-methyleneoxazolidin-2-one (6f); ^{1}H NMR (400 MHz, $CDCl_3$, 298 K) δ [ppm] = 6.85 (s, 1H), 4.65 (d, *J* = 3.4 Hz, 1H), 4.24 (d, *J* = 3.4 Hz, 1H), 1.47 (s, 6H). ^{13}C NMR (101 MHz, $CDCl_3$, 298 K) δ [ppm] = 162.21, 155.71, 84.26, 58.39, 29.38.

8. References

1. J. Dechnik, A. Nuhnen, C. Janiak, Mixed-matrix membranes of the air-stable MOF-5 analogue [Co_4 (μ_4-O)(Me_2pzba)$_3$] with a mixed-functional pyrazolate-carboxylate linker for CO_2/CH_4 separation, *Cryst. Growth Des.,* 2017, **17**, 4090-4099.
2. Y. M. Wang, K. M. Mo, X. Luo, R. Q. Xia, J. Y. Song, G. H. Ning, D. Li, An anthraquinone-based Cu(I) cyclic trinuclear complex for photo-catalyzing C-C coupling reactions, *Sci. China Chem.,* 2023, **66**, 3525–3531.
3. H. Woo, A. M. Devlin, A. J. Matzger, In Situ Observation of Solvent Exchange Kinetics in a MOF with Coordinatively Unsaturated Sites, *J. Am. Chem. Soc.,* 2023, **145**, 18634–18641.
4. (a) J. D. Chai, M. Head-Gordon, Long-range corrected hybrid density functionals with damped atom–atom dispersion corrections, *Phys. Chem. Chem. Phys*, 2008, **10**, 6615-6620.
5. K. I. Assaf, W. M. Nau, Cucurbiturils as fluorophilic receptors, *Supramol. Chem*., 2014, **26**, 657-669.
6. A. V. Marenich, C. J. Cramer, D. G. Truhlar, Universal Solvation Model Based on Solute Electron Density and on a Continuum Model of the Solvent Defined by the Bulk Dielectric Constant and Atomic Surface Tensions, *J. Phys. Chem. B,* 2009, **113**, 6378-6396.
7. J. C. Kromann, C. Steinmann, J. H. Jensen, Improving solvation energy predictions using the SMD solvation method and semiempirical electronic structure methods, *J. Chem. Phys*., 2018, **149**, 104102.
8. O. Delgado-Friedrichs, M. O'Keeffe, Identification of and Symmetry Computation for Crystal Nets. *Acta Crystallogr. Sect. A Found. Crystallogr.,* 2003, **59**, 351-360.
9. V. A. Blatov, A. P. Shevchenko, D. M. Proserpio, Applied Topological Analysis of Crystal Structures with the Program Package ToposPro. *Cryst. Growth Des.,* 2014, **14**, 3576-3586.
10. V. A. Blatov, M. O'Keeffe, D. M. Proserpio, Vertex-, Face-, Point-, Schläfli-, and Delaney-Symbols in Nets, Polyhedra and Tilings: Recommended Terminology. *CrystEngComm.,* 2010, **12**, 44-48.
11. M. O'Keeffe, M. A. Peskov, S. J. Ramsden, O. M. Yaghi, The Reticular Chemistry

Structure Resource (RCSR) Database of, and Symbols for, *Crystal Nets. Acc. Chem. Res.,* 2008, **41**, 1782-1789.

12. A. P. Shevchenko, A. A. Shabalin, I. Yu. Karpukhin, V. A. Blatov, Topological representations of crystal structures: generation, analysis and implementation in the TopCryst system. *Sci. Technol. Adv. Mater. Methods,* 2022, **2**, 250-265.
13. J. Y. Song, X. Chen, Y. M. Wang, X. Luo, T. E Zhang, G. H. Ning, D. Li, Tuning Catalytic Activity of Covalent Metal-Organic Frameworks for CO_2 Cycloaddition Reactions, *Chem. Asian J*., 2023, **18**, e202300857.
14. P. Z. Li, X. J. Wang, J. Liu, J. S. Lim, R. Zou, Y. Zhao, A Triazole-Containing Metal–Organic Framework as a Highly Effective and Substrate Size-Dependent Catalyst for CO_2 Conversion, *J. Am. Chem. Soc*., 2016, **138**, 2142-2145.
15. P. Z. Li, X. J. Wang, J. Liu, H. S. Phang, Y. Li, Y. Zhao, Highly Effective Carbon Fixation via Catalytic Conversion of CO_2 by an Acylamide-Containing Metal–Organic Framework, *Chem. Mater*., 2017, **29**, 9256-9261.
16. N. Seal, S. Neogi, Intrinsic-Unsaturation-Enriched Biporous and Chemorobust Cu(II) Framework for Efficient Catalytic CO_2 Fixation and Pore-Fitting Actuated Size-Exclusive Hantzsch Condensation with Mechanistic Validation, *ACS Appl. Mater. Interfaces,* 2021, **13**, 55123-55135.
17. J. Gu, X. Sun, X. Liu, Y. Yuan, H. Shan, Y. Liu, Highly efficient synergistic CO_2 conversion with epoxide using copper polyhedron-based MOFs with Lewis acid and base sites, *Inorg. Chem. Front*., 2020, **7**, 4517-4526.
18. W. M. Wang, W. T. Wang, M. Y. Wang, A. L. Gu, T. D. Hu, Y. X. Zhang, Z. L. Wu, A Porous Copper–Organic Framework Assembled by [Cu_{12}] Nanocages: Highly Efficient CO_2 Capture and Chemical Fixation and Theoretical DFT Calculations, *Inorg. Chem.,* 2021, **60**, 9122-9131.
19. X. Yu, J. Gu, X. Liu, Z. Chang, Y. Liu, Exploring the Effect of Different Secondary Building Units as Lewis Acid Sites in MOF Materials for the CO_2 Cycloaddition Reaction, *Inorg. Chem*., 2023, **62**, 11518-11527.
20. K. Huang, Q. Li, X. Y. Zhang, D. B. Qin, B. Zhao, Copper-Cluster-Based MOF as a Heterogeneous Catalyst for CO_2 Chemical Fixation and Azide–Alkyne Cycloaddition, *Cryst. Growth Des.,* 2022, **22**, 6531-6538.

21. J. Tapiador, P. Leo, F. Gándara, G. Calleja, G. Orcajo, Robust Cu-URJC-8 with mixed ligands for mild CO_2 cycloaddition reaction, *J. CO_2 Util*., 2022, **64**, 102166.
22. Y. Y. Zhao, L. Chen, Z. Xu, C. Y. Zhu, P. Li, W. Gao, J. Y. Li, X. M. Zhang, Microporous Cd-MOF as multifunctional material for rapid and visual luminescence sensing of Fe^{3+}, MnO_4^- and TNP in water and efficient CO_2 catalytic conversion, *Micropor. Mesopor. Mat.,* 2023, **362**, 112764.
23. R. Das, D. Muthukumar, R. S. Pillai, C. M. Nagaraja, Rational Design of a Zn^{II} MOF with Multiple Functional Sites for Highly Efficient Fixation of CO_2 under Mild Conditions: Combined Experimental and Theoretical Investigation, *Chem. Eur. J.,* 2020, **26**, 17445-17454.
24. N. Sharma, S. S. Dhankhar, C. M. Nagaraja, A Mn(II)-porphyrin based metal-organic framework (MOF) for visible-light-assisted cycloaddition of carbon dioxide with epoxides, *Micropor. Mesopor. Mat.,* 2019, **280**, 372-378.
25. G. Jin, D. Sensharma, N. Zhu, S. Vaesen, W. Schmitt, A highly augmented, (12,3)-connected Zr-MOF containing hydrated coordination sites for the catalytic transformation of gaseous CO_2 to cyclic carbonates, *Dalton Trans*., 2019, **48**, 15487-15492.
26. H. Chen, L. Fan, X. Zhang, L. Ma, Nanocage-Based $In^{III}\{Tb^{III}\}_2$-organic framework featuring lotus shaped channels forhighly efficient CO_2 fixation and I_2 capture, *ACS Appl. Mater. Interfaces,* 2020, **12**, 27803-27811.
27. H. Chen, L. Fan, X. Zhang, Highly robust 3s-3d {CaZn}-organic framework for excellent catalytic performance on chemical fixation of CO_2 and Knoevenagel Condensation Reaction, *ACS Appl. Mater. Interfaces*, 2020, **12**, 54884-54892.
28. A. Gogia, S. K. Mandal, Topologically driven pore/surface engineering in a recyclable microporous metal-organic vessel decorated with hydrogen-bond acceptors for solvent-free heterogeneous catalysis, *ACS Appl. Mater. Interfaces*, 2022, **14**, 27941-27954.
29. Y. Li, X. Zhang, J. Lan, D. Li, Z. Wang, P. Xu, J. Sun, A high-performance zinc-organic framework with accessible open metal sites catalyzes CO_2 and styrene oxide into styrene carbonate under mild conditions, *ACS Sustainable Chem. Eng.,* 2021, **9**, 2795-2803.

30. G. Chakraborty, P. Das, S. K. Mandal, Efficient and highly selective CO_2 capture, separation, and chemical conversion under ambient conditions by a polar-group appended copper(II) metal-organic framework, *Inorg. Chem.,* 2021, **60**, 5071-5080.
31. V. Gupta, S. K. Mandal, Effect of unsaturated metal site modulation in highly stable microporous materials on CO_2 capture and fixation, *Inorg. Chem.,* 2022, **61**, 3086-3096.
32. B. B. Lu, W. Jiang, J. Yang, Y. Y. Liu, J. F. Ma, Resorcin [4] arene-based microporous metal-organic framework as an Efficient catalyst for CO_2 cycloaddition with epoxides and highly selective luminescent sensing of $Cr_2O_7^{2-}$, *ACS Appl. Mater. Interfaces,* 2017, **9**, 39441-39449.
33. A. Liu, Y. Chen, P. Liu, W. Qi, B. Li, Conversion of CO_2 to epoxides or oxazolidinones enabled by a Cu^I/Cu^{II}-organic framework bearing a tri-functional linker, *Inorg. Chem. Front.,* 2022, **9**, 4425-4432.
34. P. Rani, A. Husain, K. K. Bhasin, G. Kumar, Metal-organic framework-based selective molecular recognition of organic amines and fixation of CO_2 into cyclic carbonates, *Inorg. Chem.,* 2022, **61**, 6977-6994.
35. X. Zhao, B. B. Qin, T. He, H. P. Wang, J. Liu, Stable Pyrene-Based Metal–Organic Framework for Cyclization of Propargylic Amines with CO_2 and Detection of Antibiotics in Water, *Inorg. Chem.,* 2023, **62**, 18553-18562.
36. A. L. Gu, Y. X. Zhang, Z. L. Wu, H. Y. Cui, T. D. Hu, B. Zhao, Highly Efficient Conversion of Propargylic Alcohols and Propargylic Amines with CO_2 Activated by Noble-Metal-Free Catalyst Cu_2O@ZIF-8, *Angew. Chem. Int. Ed.,* 2022, **61**, e202114817.
37. C. S. Cao, S. M. Xia, Z. J. Song, H. Xu, Y. Shi, L. N. He, P. Cheng, B. Zhao, Highly Efficient Conversion of Propargylic Amines and CO_2 Catalyzed by Noble-Metal-Free $[Zn_{116}]$ Nanocages, *Angew. Chem. Int. Ed*., 2020, **59**, 8586-8593.
38. G. Zhang, H. Yang, H. Fei, Unusual Missing Linkers in an Organosulfonate-Based Primitive–Cubic (pcu)-Type Metal–Organic Framework for CO_2 Capture and Conversion under Ambient Conditions, *ACS Catal*., 2018, **8**, 2519-2525.
39. W. M. Wang, N. Qiao, J. L. Wang, Y. Chen, J. C. Yan, C. Y. Xu, C. S. Cao, A $[Cu_2I_2]$ cluster-based lanthanide metal–organic framework (MOF) catalyst for the highly

efficient conversion of CO_2 with propargylic alcohols and aziridines, *Catal. Today,* 2024, **425**, 114359.

40. H. Y. Cui, Y. X. Zhang, C. S. Cao, T. D. Hu, Z. L. Wu, Engineering noble-metal-free metal–organic framework composite catalyst for efficient CO_2 conversion under ambient conditions, *Chem. Eng. J*., 2023, **451**, 138764.
41. X. L. Jiang, Y. E Jiao, S. L. Hou, L. C. Geng, H. Z. Wang, B, Zhao, Green Conversion of CO_2 and Propargylamines Triggered by Triply Synergistic Catalytic Effects in Metal–Organic Frameworks, *Angew. Chem*., 2021, **133**, 20580-20586.

^{1}H NMR and ^{13}C NMR spectra of compounds 4 and 6

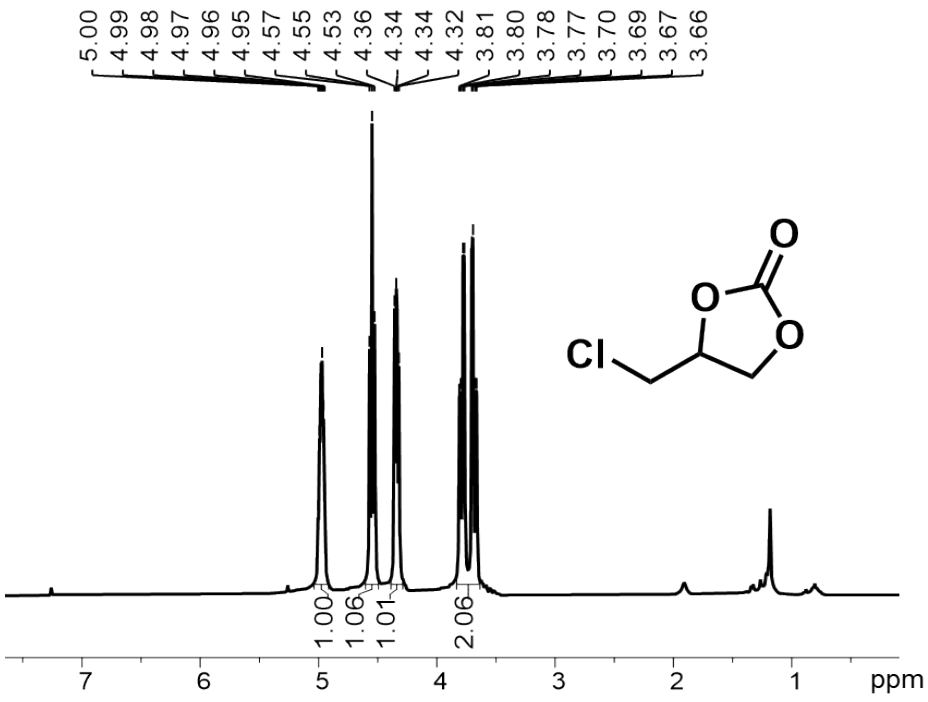

^{1}H NMR spectrum (400 MHz, $CDCl_3$, 298 K) of compound **4a**.

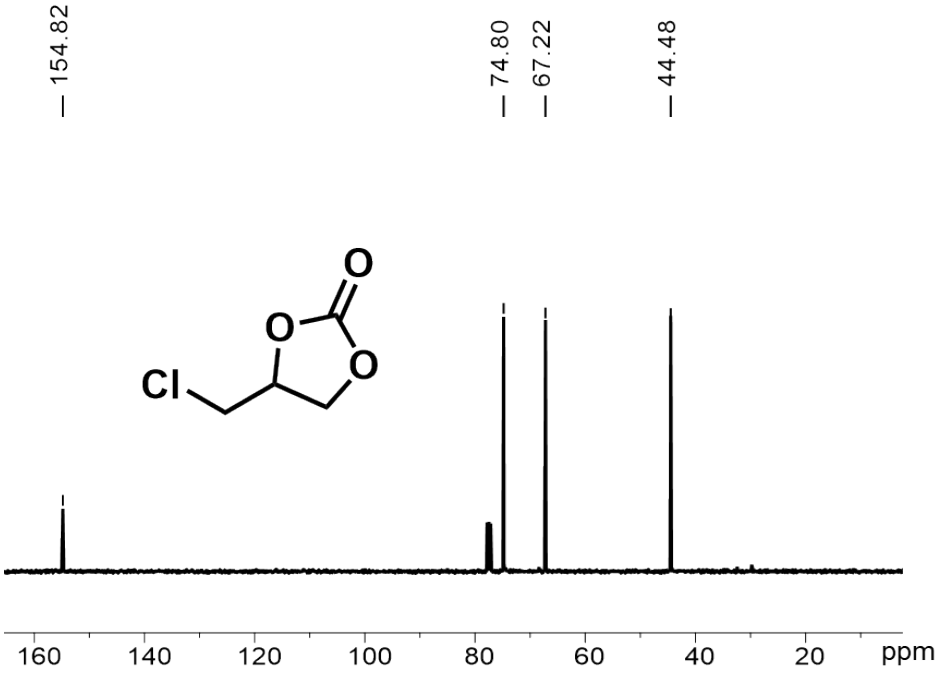

^{13}C NMR spectrum (101 MHz, $CDCl_3$, 298 K) of compound **4a**.

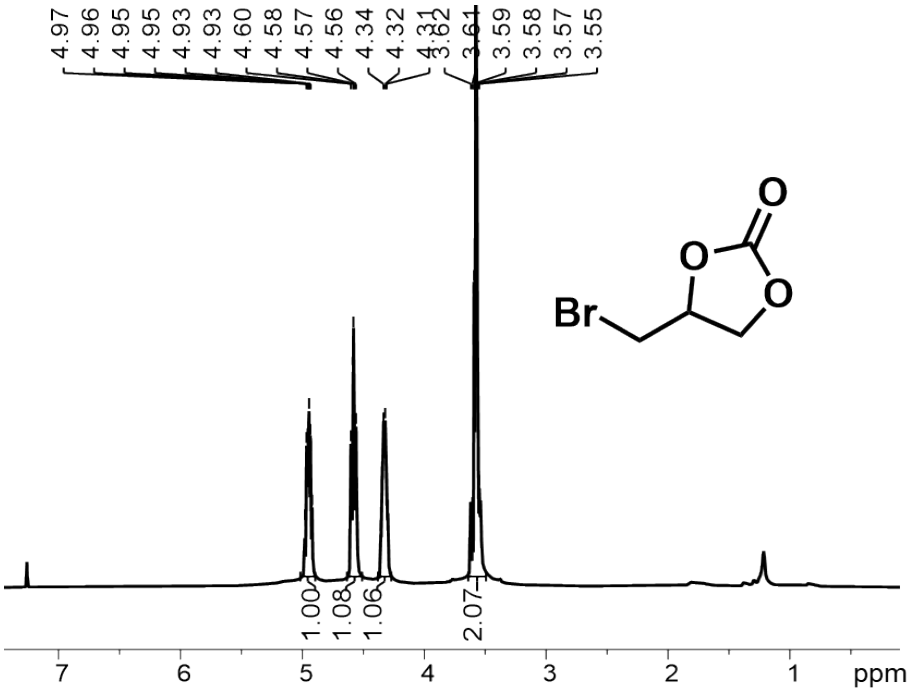

^{1}H NMR spectrum (400 MHz, $CDCl_3$, 298 K) of compound **4b**.

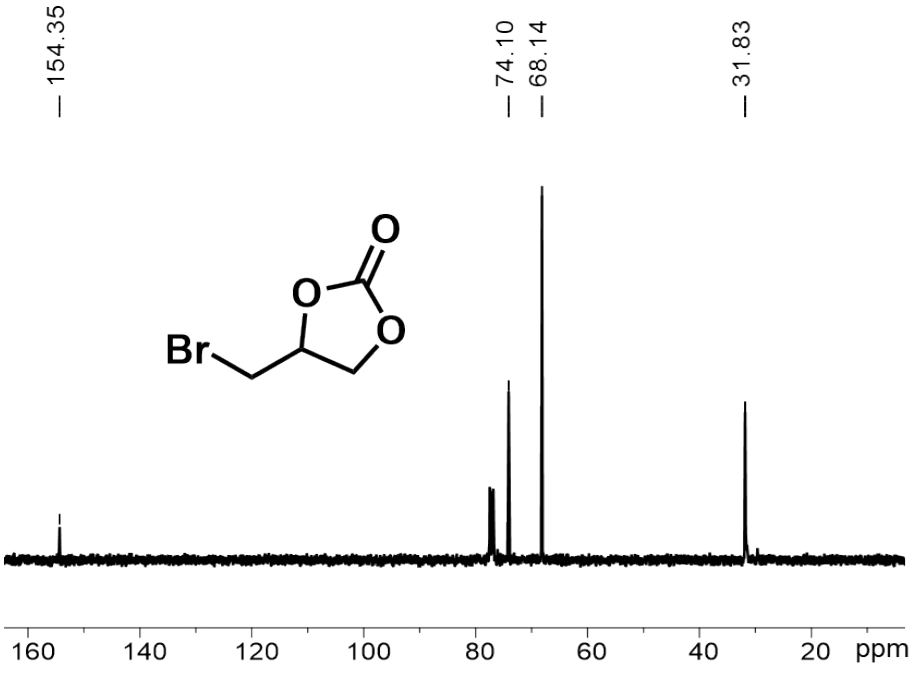

^{13}C NMR spectrum (101 MHz, $CDCl_3$, 298 K) of compound **4b**.

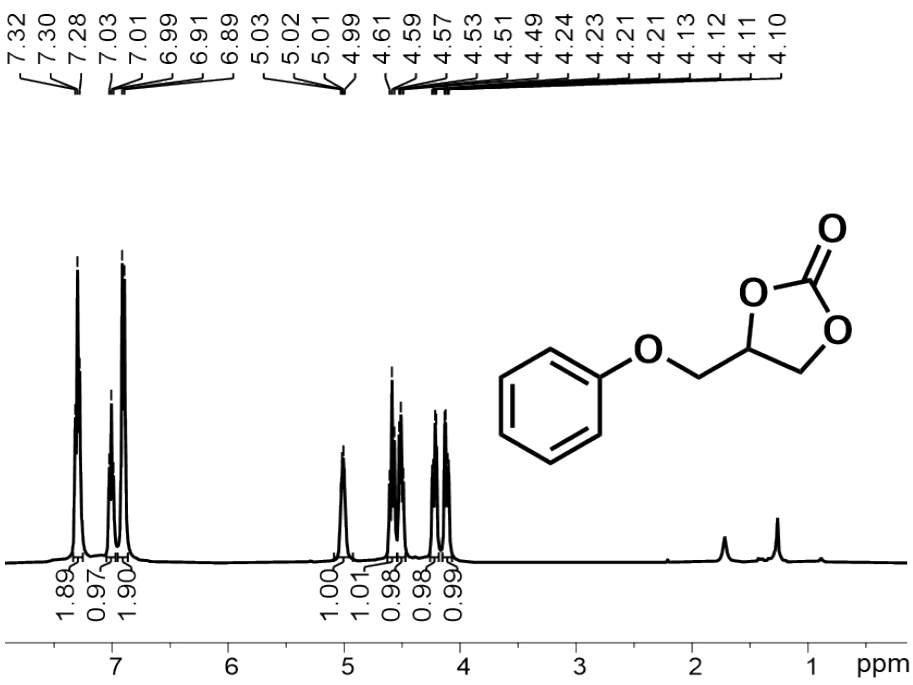

^{1}H NMR spectrum (400 MHz, $CDCl_3$, 298 K) of compound **4c**.

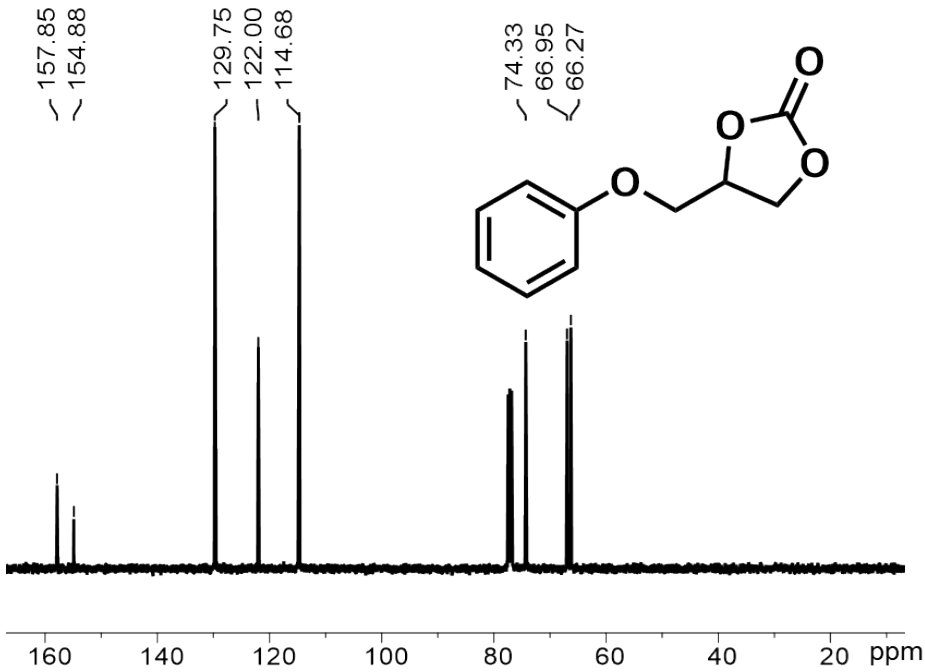

^{13}C NMR spectrum (101 MHz, $CDCl_3$, 298 K) of compound **4c**.

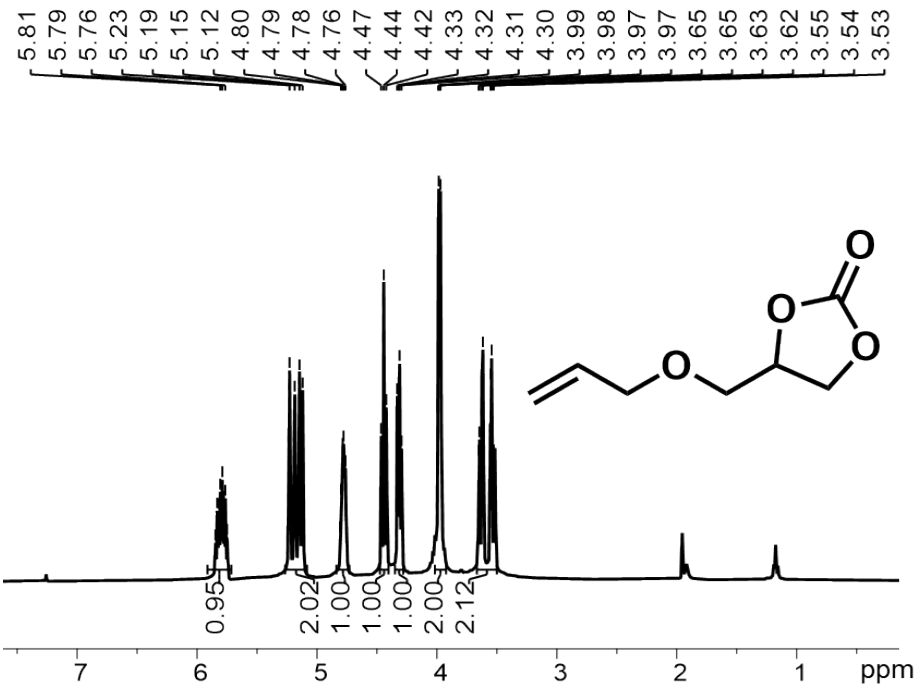

^{1}H NMR spectrum (400 MHz, $CDCl_3$, 298 K) of compound **4d**.

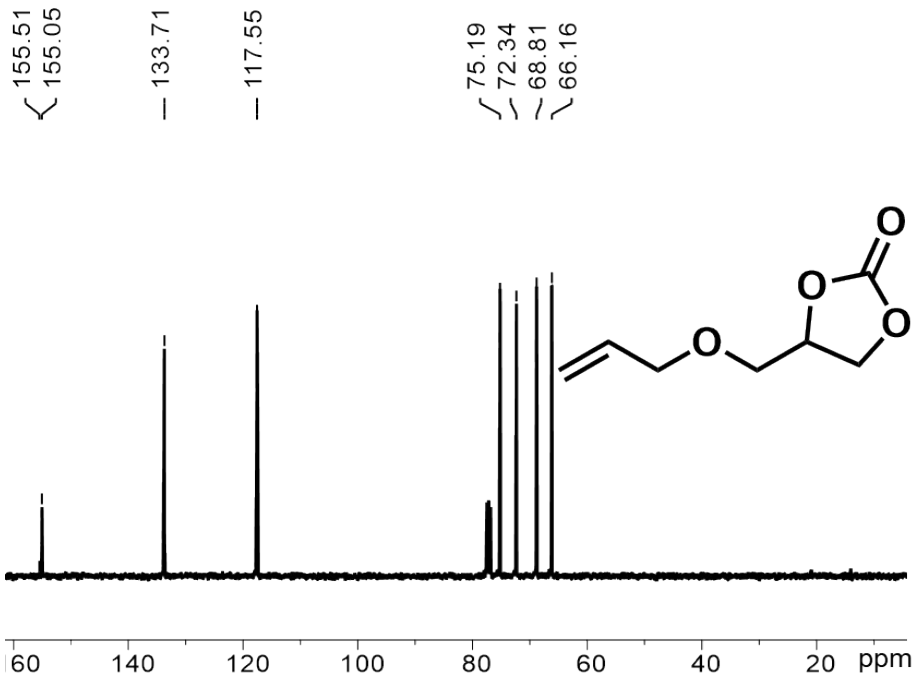

^{13}C NMR spectrum (101 MHz, $CDCl_3$, 298 K) of compound **4d**.

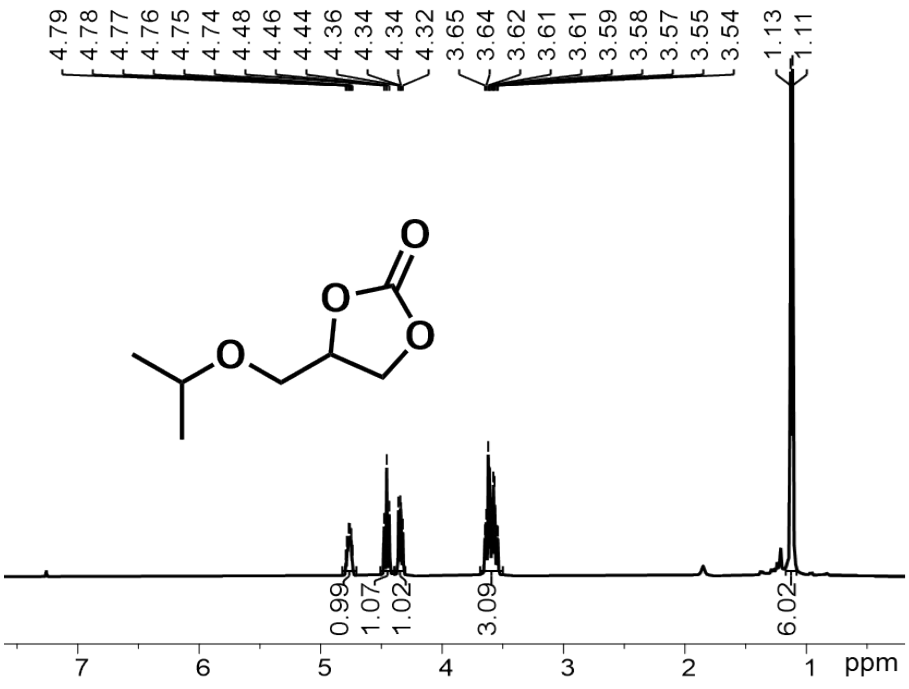

^{1}H NMR spectrum (400 MHz, $CDCl_3$, 298 K) of compound **4e**.

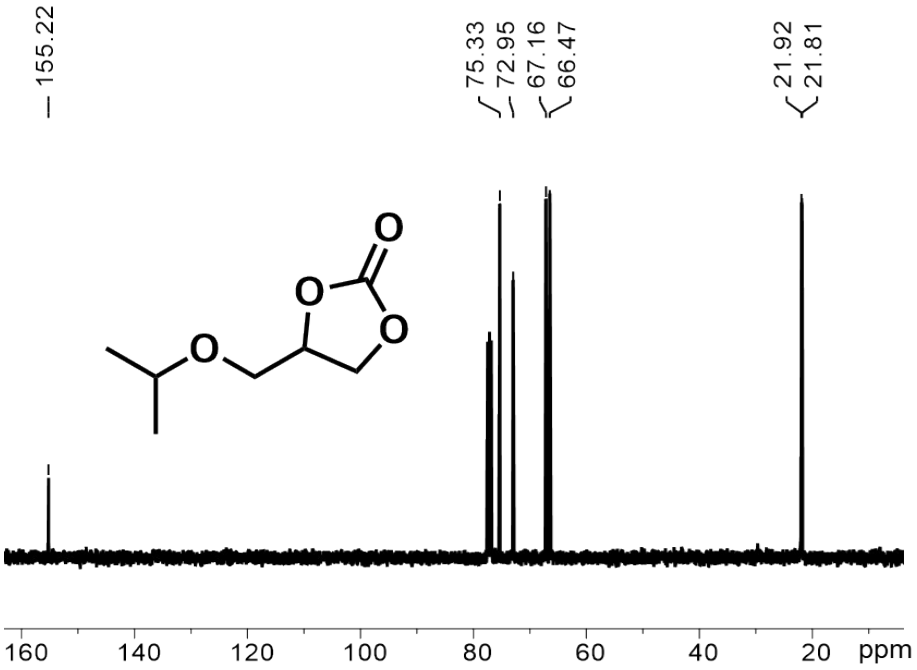

^{13}C NMR spectrum (101 MHz, $CDCl_3$, 298 K) of compound **4e**.

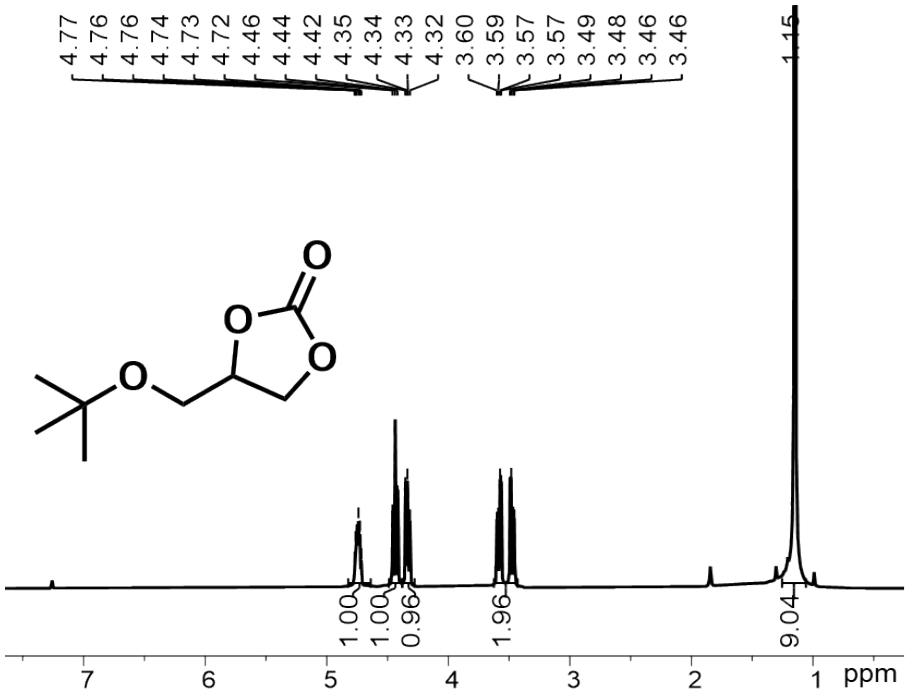

^{1}H NMR spectrum (400 MHz, $CDCl_3$, 298 K) of compound **4f**.

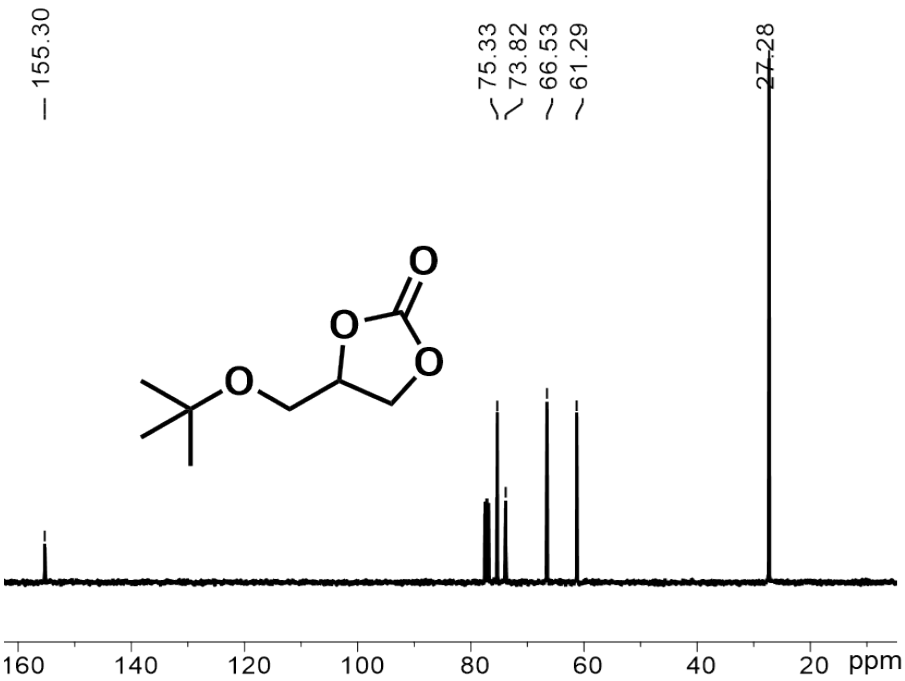

^{13}C NMR spectrum (101 MHz, $CDCl_3$, 298 K) of compound **4f**.

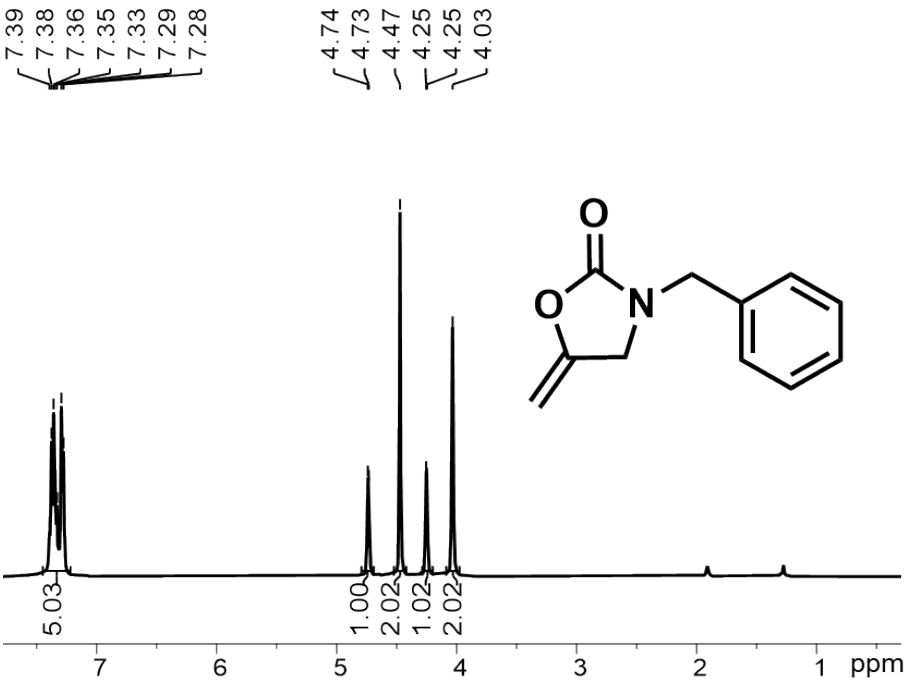

^{1}H NMR spectrum (400 MHz, $CDCl_3$, 298 K) of compound **6a**.

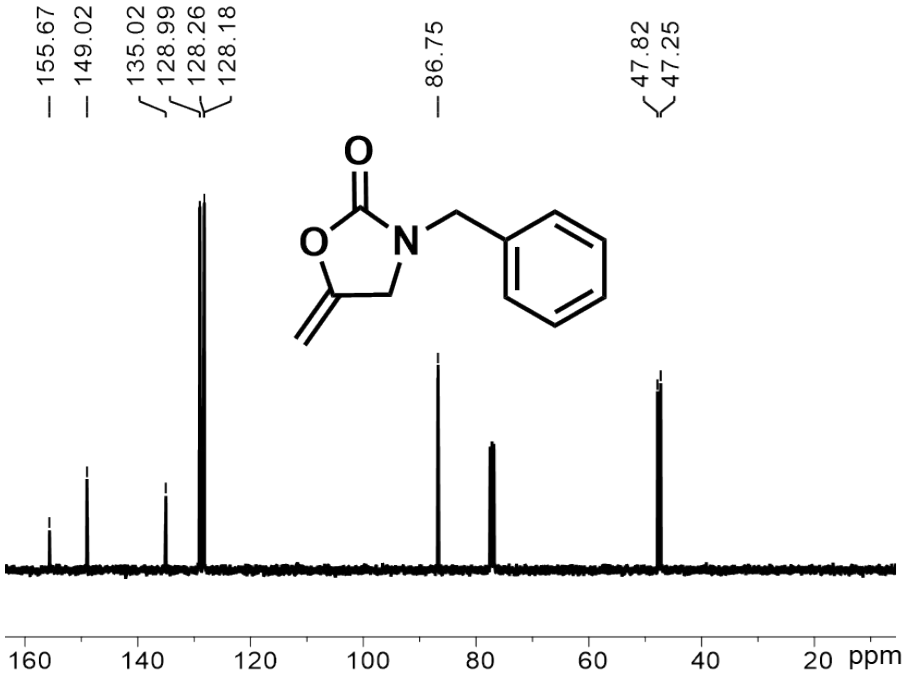

^{13}C NMR spectrum (101 MHz, $CDCl_3$, 298 K) of compound **6a**.

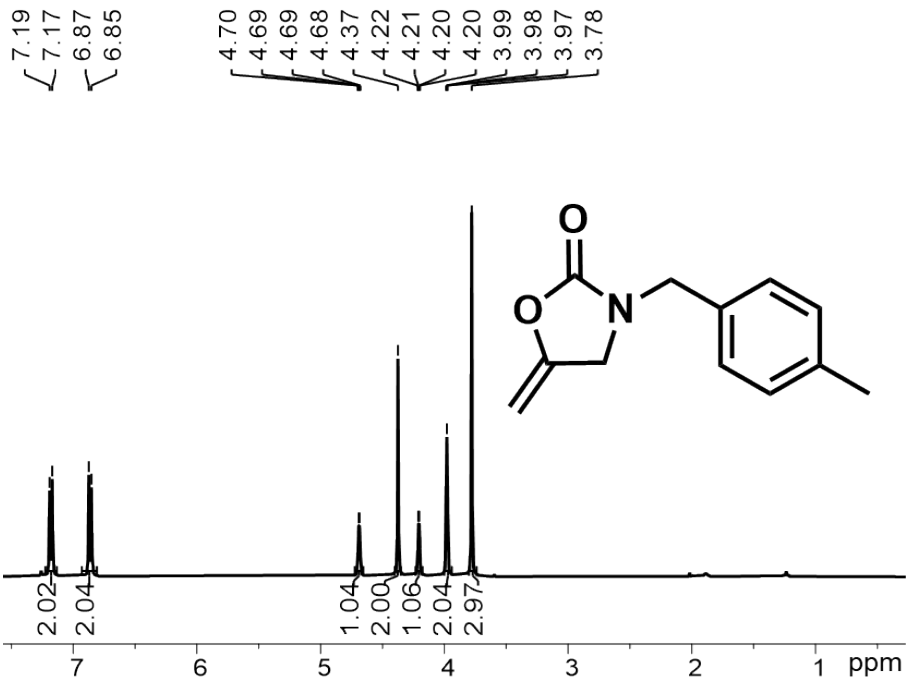

^{1}H NMR spectrum (400 MHz, $CDCl_3$, 298 K) of compound **6b**.

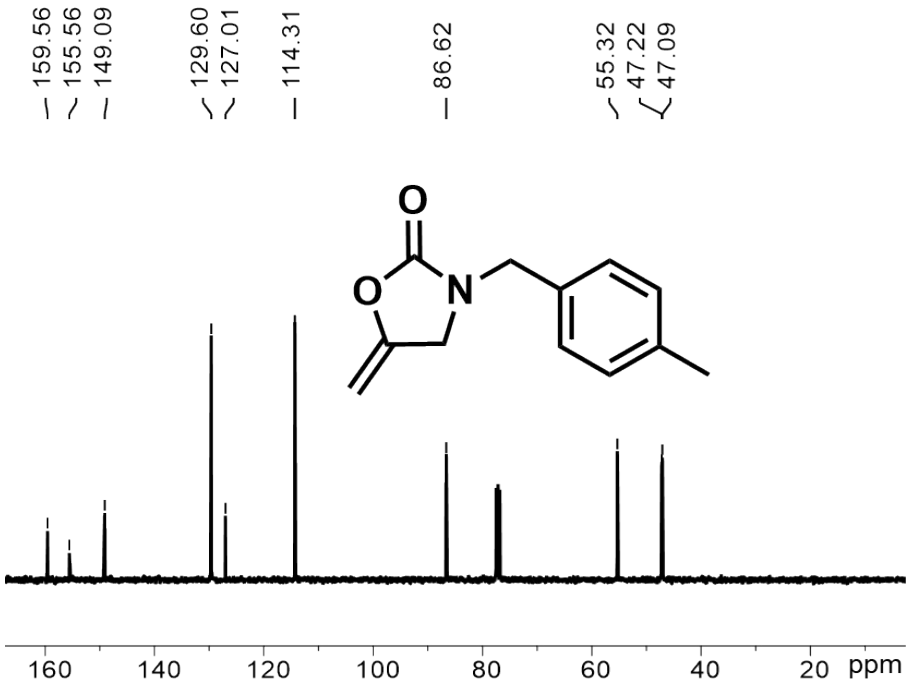

^{13}C NMR spectrum (101 MHz, $CDCl_3$, 298 K) of compound **6b**.

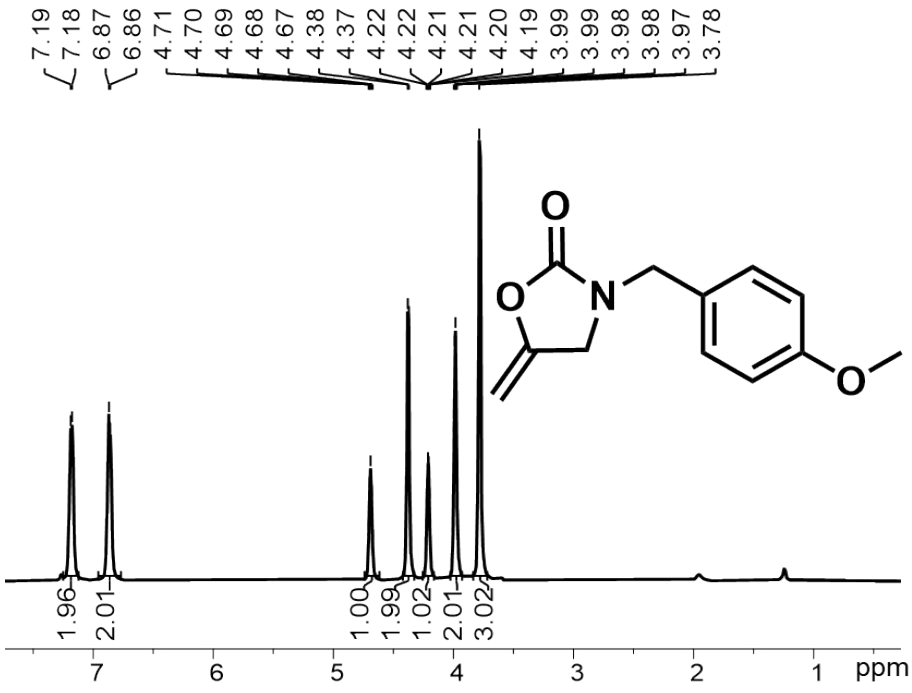

^{1}H NMR spectrum (400 MHz, $CDCl_3$, 298 K) of compound **6c**.

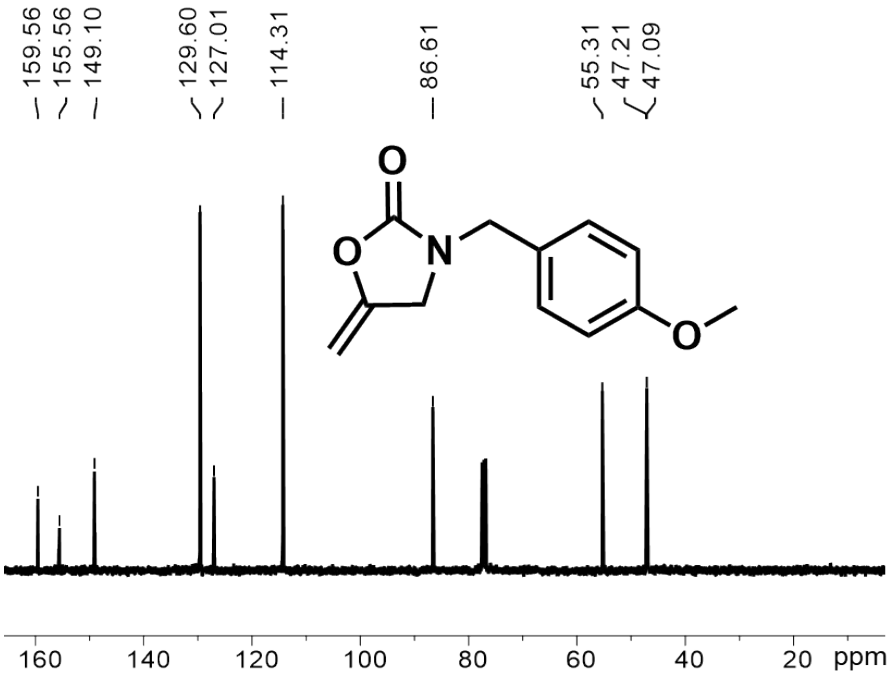

^{13}C NMR spectrum (101 MHz, $CDCl_3$, 298 K) of compound **6c**.

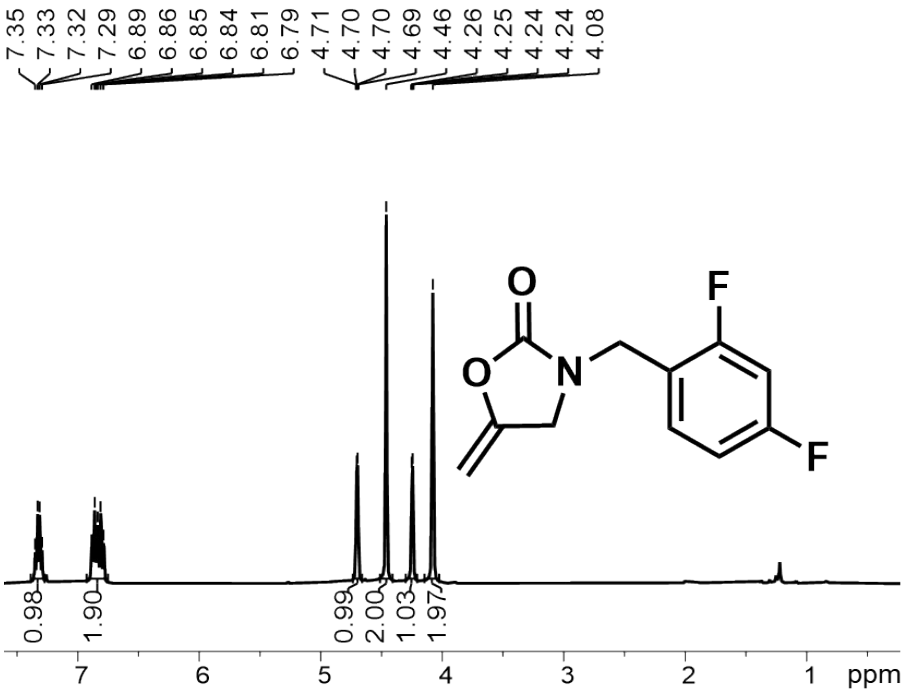

^{1}H NMR spectrum (400 MHz, $CDCl_3$, 298 K) of compound **6d**.

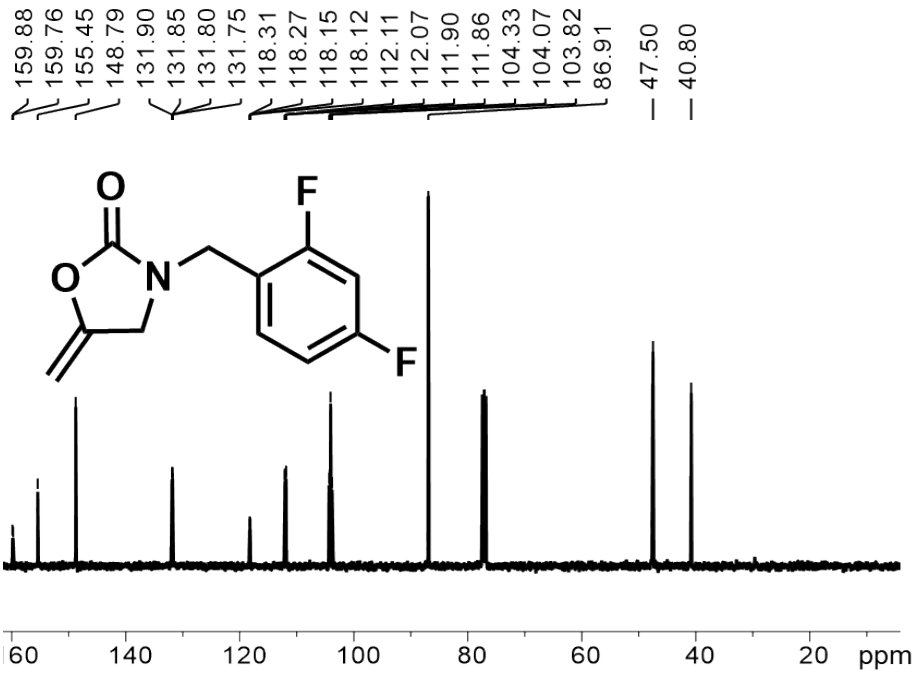

^{13}C NMR spectrum (101 MHz, $CDCl_3$, 298 K) of compound **6d**.

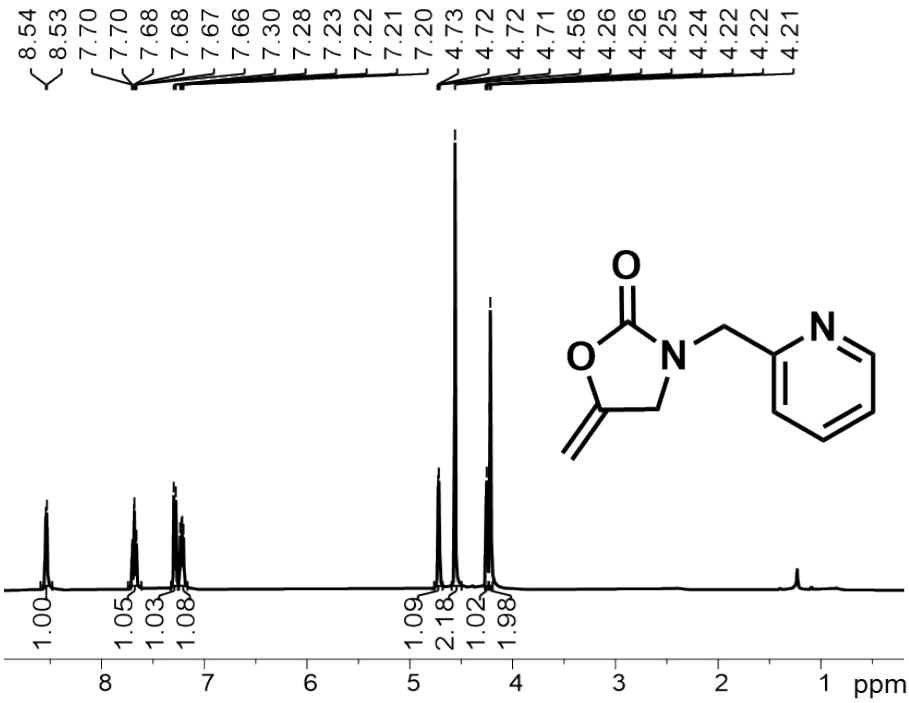

^{1}H NMR spectrum (400 MHz, $CDCl_3$, 298 K) of compound **6e**.

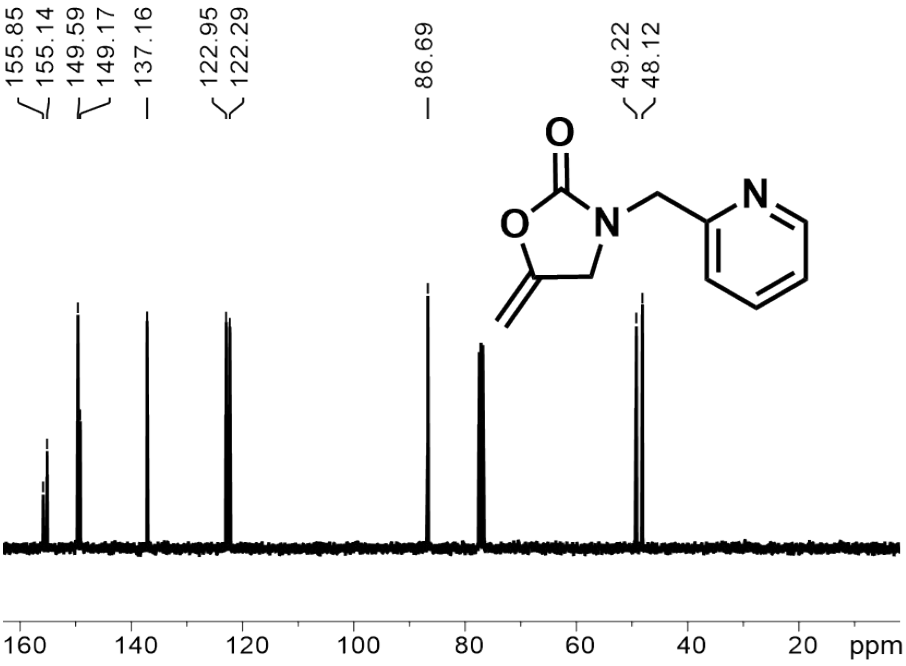

^{13}C NMR spectrum (101 MHz, $CDCl_3$, 298 K) of compound **6e**.

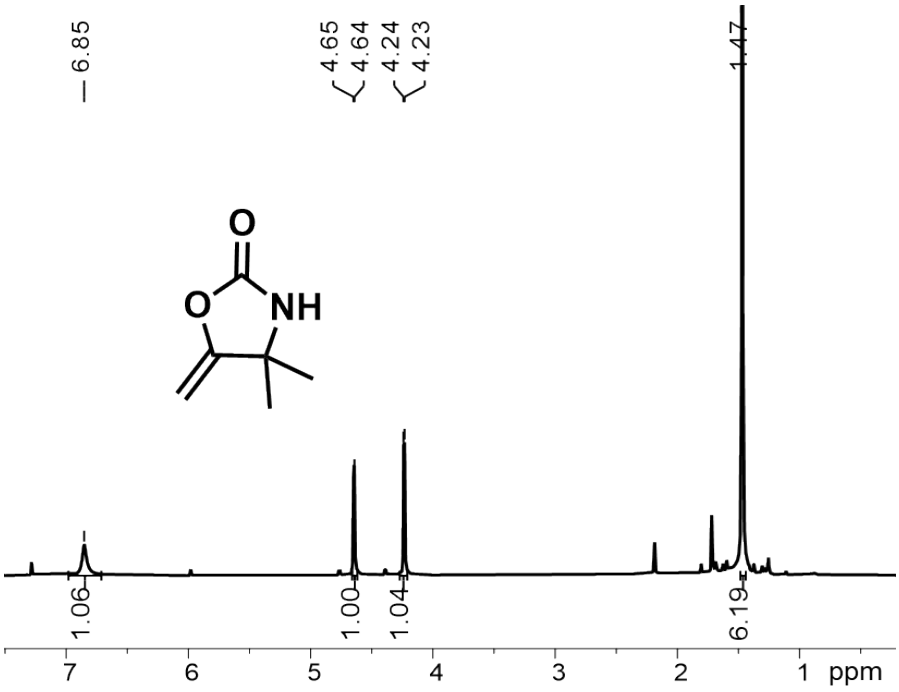

^{1}H NMR spectrum (400 MHz, $CDCl_3$, 298 K) of compound **6f**.

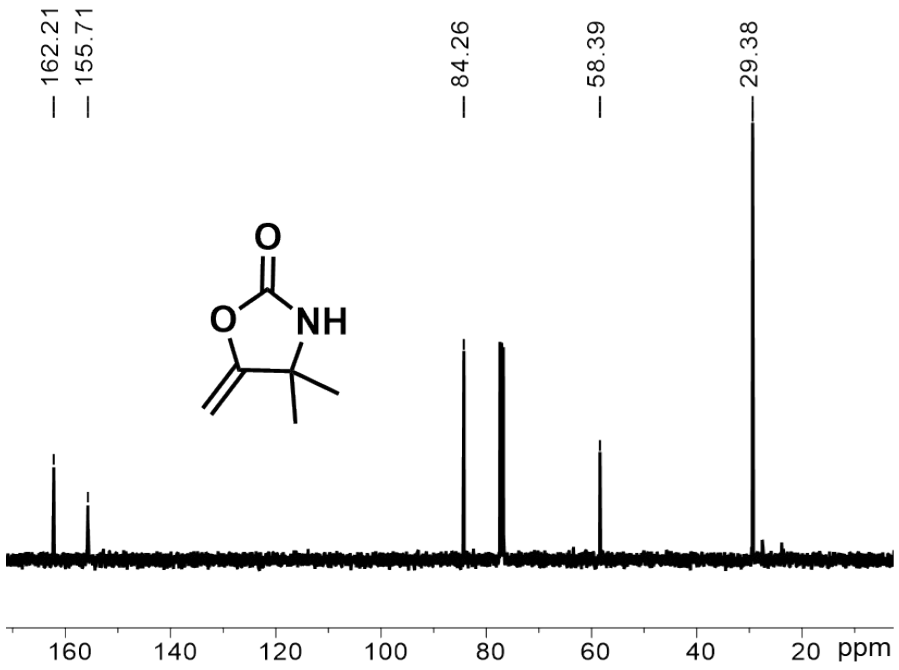

^{13}C NMR spectrum (101 MHz, $CDCl_3$, 298 K) of compound **6f**.